Antenna and Plasmonic Properties of Scanning Probe Tips at Optical and Terahertz Regimes

A. Haidary*, Y. Miyahara, and P. Grütter
Department of Physics, Faculty of Science, McGill University, Montreal, Canada
* abutaleb.haidary@mcgill.ca

Abstract: Electric field enhancement (γ) at the end of a sharp tip is calculated by finite-element method (FEM). The metal tip is modeled as a 3-D gold hemi-ellipsoid illuminated by two different excitation frequencies in the optical and Terahertz (THz) regimes with the wavelengths of 630 nm and 0.3 mm, respectively. The dependence of field enhancement on apex radius, tip geometry, radiation wavelengths, tip and sample materials at optical and THz regimes is investigated. First, Maxwell's equations are solved in the frequency domain and the reliability of FEM method is validated by comparing the results with analytical solutions and the finite element time domain method. Our calculation shows the competition between antenna and plasmon resonances and associated dephasing effects for the field enhancement at optical and THz regimes. When the size of the metal tip is larger than approximately 0.4λ (λ is the radiation wavelength), the field enhancement is less than 10 for λ=630 due to the dephasing effects whereas at λ=0.3 mm (THz radiation) the antenna effect is dominant leading to an extremely high field enhancement.

Keywords: Electric field enhancement, scanning probe tips, antenna resonance, plasmon resonance, THz electric field enhancement, dephasing effects.

1. Introduction

Recent developments in nanotechnology have increased the demands for analytical and numerical tools to investigate the properties of materials at nano-scale. Scanning probe microscopy (SPM) has significantly advanced the way we look at the material surface properties at the nano-scale. Scanning near-field optical microscopy (SNOM) can provide simultaneous topographical and optical information about the sample with a resolution substantially below 100 nm. With this technique the sub wavelength-sized metal tip captures incident optical/THz waves and converts them into confined near fields at the tip apex. The confined electric fields are scattered off the metal tip which is held close to a surface. The scattered radiation carries information on the dielectric properties of the sample [1].

Tip Enhanced Raman Spectroscopy (TERS) is another useful technique which is based on the extremely high enhancement of the electric field (E) at the apex of a metallic tip when excited with visible electromagnetic waves [2]. TERS provides the opportunity for chemically specific scanning probe microscopy. Raman signal intensity will be enhanced by a factor proportional to the forth power of the enhancement of the local incident near field, i.e., E^4 [3]. Thus small variations in the electric field intensity will induce dramatic change in the Raman signal. Therefore, it is necessary to determine which parameters are important for controlling the enhancement of electric field in order to obtain the maximum field enhancement.

Electric field enhancement and its spatial distribution have been investigated for a variety of tip geometries and tip-sample materials using different theoretical methods at optical regimes [4-11]. Electromagnetic wave scattered from spherical nanoparticles can be solved analytically using Mie's theory [12]. It is extended for other simple geometries by replacing Maxwell's equations with the Laplace equation considering quasistatic approximation which provides the electrostatic potential and thus the distribution of the local optical electric field at the apex region [4]. However, this method is inaccurate for particle sizes larger than 20 nm at optical wavelengths as the dephasing effects become significant [14]. The accurate theoretical treatment of the problem is possible by solving Maxwell's equations numerically [13].

The work described here is based on FEM using COMSOL Multiphysics. First, Maxwell's equations are solved in the frequency domain for a gold tip and glass substrate and then the results

Excerpt from the Proceedings of the 2014 COMSOL Conference in Boston

are compared with analytical solutions to cross check our modeling. Then we study the effect of tip apex radius, substrate and radiation wavelengths on the field enhancement. Furthermore, we investigate the relative importance of two different underlying physical origins of the field enhancement i.e. antenna and plasmonic resonances at optical and THz regimes.

2. Methods

In the present work, tetrahedral (first order) mesh elements are used to solve Maxwell's equations in the frequency domain to calculate local field enhancement at the end of a 3-D gold hemi-ellipsoid tip and a glass substrate with tip-sample distance of 5 nm and apex radius of 10 nm (figure. 1). The solutions of Maxwell's equations at each element are stitched together and give the magnitude of electric field for the original full size problem. First, an electromagnetic wave incident to the metal tip is modeled by a plane wave field polarized parallel to the tip axis in the optical regime with the wavelength of 630 nm. The result is compared with the quasistatic approximation by solving the Laplace equation analytically [4] as well as a finite–element time-domain (FETD) approach [14]. Our calculations show a very good agreement with both analytical theory and FETD calculations.

This gives us confidence in the reliability and accuracy of our calculations to investigate a 3-D gold hemi-ellipsoid compressed in the xz plane (Figure 2) with and without considering substrates, and allowing us to study the effect of apex radius and substrate on the enhancement of the electric field. We compare results for optical and THz excitation frequency to investigate field enhancement in the THz regime.

In the last part, a gold shaft is added to the 3-D hemi-ellipsoid gold tip (Figure 3). By increasing the height of the metallic shaft, the antenna, plasmonic and dephasing effects of the tip are investigated.

The plasmonic behavior of the tip is explicitly taken into account by considering the frequency dependence of complex dielectric functions of three different mediums.

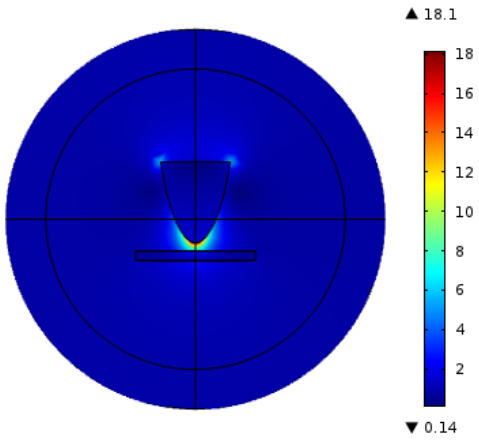

Figure 1. Spatial distribution and field enhancement for Au tip and glass substrate with tip-sample separation of 5 nm. The apex radius for Au tip is 10 nm. Field enhancement at 0.125 nm above the glass surface is 7.5 for λ=630 nm.

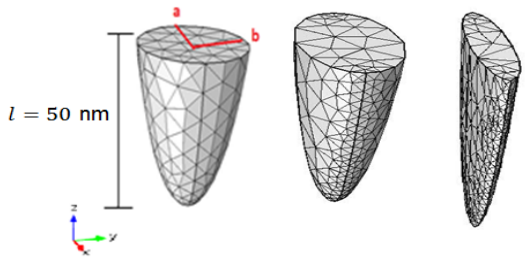

Figure 2. 3-D hemi-ellipsoid metal tip apex with the height of 50 nm compressed in xz plane. When compressed, the tip apex radius in the xz plane is kept constant (10 nm) and the apex radius in the yz plane is varying.

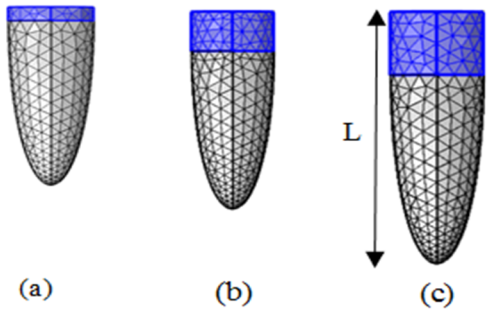

Figure 3. Au shaft is added to the 3-D hemi-ellipsoid metal tip apex with the apex radius of 10 nm. The height of hemi-ellipsoid without the gold shaft is 120 nm. The blue color represents the Au shaft with a height of a) 10 nm b) 30 nm and c) 40 nm.

2. Theory

Theoretical studies identified two main mechanisms to explain field enhancement at the end of a sharp tip.

2.1 Antenna resonance

According to the IEEE definition, an antenna is a part of a transmitting or receiving system that is designed to radiate or to receive electromagnetic waves. Antenna radiation has strong geometrical dependence. Thus, for it to be efficient, it must have a physical extent that is at least an appreciable fraction of a wavelength at the operating frequency [15].
For a thin wire, the maximum field enhancement due to antenna effect can be reached when the length of the wire approximately equals an odd integer multiple of half a wavelength ($L = n\lambda + \lambda/2$), with $n = 1,2,\ldots$) [15]. Analytical solutions to calculate electric field enhancement for a small metallic ellipsoid in the presence of an external field is given by [16]. The expression for the field enhancement factor (γ) is [16]

$$\gamma = \left|\frac{\varepsilon}{1+(\varepsilon-1)A}\right| \qquad (1)$$

where ε and A are a complex dielectric constant and the depolarization factor for a full ellipsoid, respectively. The latter is given by:

$$A(r) = \frac{1}{2r^2}\int_0^{\infty}\frac{1}{(s+1)^{\frac{3}{2}}\,(s+r^{-2})}\,ds \qquad (2)$$

where $r = l_x/l_y$ is the ratio of long to short axis of elongated ellipsoid.

Martin et al [14] investigated antenna resonance of a full ellipsoid by using FETD calculations. It is shown how the electric fields are increased when the length of the ellipsoid matches the phase of propagation. Moreover, the dephasing effects decrease γ substantially when the ellipsoid becomes lager than $\lambda/2$.

2.2 Plasmon resonance

Surface plasmons are collective oscillations of the conduction electrons at metal surfaces. For a particle much smaller than the wavelength of the excitation, all but the dipolar plasmon can be ignored. When the exciting light is in resonance with the dipolar plasmon, the metal particle/tip will radiate light characteristic of dipolar radiation [3].
Field enhancement for metals such as gold and silver is mostly due to plasmon resonance, whereas the antenna effect provides a negligible contribution to the field enhancement at visible wavelengths.
Plasmon resonance occurs for a small ellipsoid or sphere when the denominator of equation (1) becomes zero.

$$Re\,[1+(\varepsilon-1)A] = 0 \qquad (3)$$

For a small gold ellipsoid, the plasmon resonance is found when the aspect ratio of the ellipsoid equals to r =3.2 at λ =633 nm using FETD calculations [14]. Furthermore, when the length of the ellipsoid is larger than $\lambda/2$, plasmon resonance becomes ineffective due to dephasing effects resulting in a small γ.

3. Use of COMSOL Multiphysics

In order to solve a high-frequency electromagnetic problem, the RF module of COMSOL Multiphysics is used. Maxwell's equations are solved in the frequency domain as;

$$\nabla\times(\mu_r^{-1}\times\boldsymbol{E}) - k_0^2\left(\varepsilon_r - \frac{j\sigma}{\omega\varepsilon_0}\right)\boldsymbol{E} = 0 \qquad (4)$$

Where ω, μ_r, ε_r and σ are excitation frequency, relative permeability, relative permittivity and electrical conductivity respectively.
The electromagnetic plane-wave is polarized parallel to the metal tip to represent an incident laser beam. The magnitude of the incident laser electric field is set to 1; thus, the magnitude of the computed scattered electric field is equivalent to the electric field enhancement.
The whole system is surrounded by a spherical boundary to separate the finite mesh volume from the infinite open domain. The outer layer of the spherical geometry is set as a perfectly matched

layer (PML) to absorb all the outgoing wave energy without any impedance mismatch.
Resolving the skin depth is one of the most important requirements when dealing with high frequency simulation which is a function of excitation frequency, permeability and conductivity of the material. In this work, the skin depth is treated by using a Boundary Layer mesh. The whole system is meshed by using User-controlled mesh with a minimum mesh element of 10 nm for the tip apex.
The parameters for this simulation are the complex frequency-dependent dielectric functions of the tip, the substrate and the medium between the metal tip and substrate, as well as tip apex radius. The complex dielectric functions, which depend on the material and the excitation laser wavelength, are assumed to be homogeneous within the boundaries of the metallic tip and substrate. The medium between the gold metal tip and the substrate is considered to be vacuum.

4. Results and Discussion

4.1 Effect of tip apex radius with and without substrate on the field enhancement.

Figures 4 and 5 show dependence of the field enhancement on the tip apex radius (figure 2). The field enhancement is calculated near the Au tip apex at 0.125 nm below the tip apex as well as near the glass substrate at 0.125 nm above the surface plane at optical and THz regimes with the wavelength of 630 nm and 0.3 mm with the corresponding dielectric function as $\varepsilon_{Optic} = -9.90 + 1.05\,i$ [4] and $\varepsilon_{THz} = -1.4 \times 10^5 + 1.6 \times 10^6\,i$ [17] respectively. First, the field enhancement for the Au tip is calculated (tip without substrate). Then, by adding a glass substrate to the model with a tip-sample distance of 5 nm, field enhancement is calculated near the apex region of the Au tip (tip with substrate), as well as near the sample surface.
Our results show a non-linear dependence of the field enhancement near the tip apex and substrate in the optical visible regime. The field enhancement is increased by adding the glass substrate which is due to the optical coupling between the Au tip and substrate. The lateral confinement of the field enhancement in the tip-sample gap is dependent on the sample material.

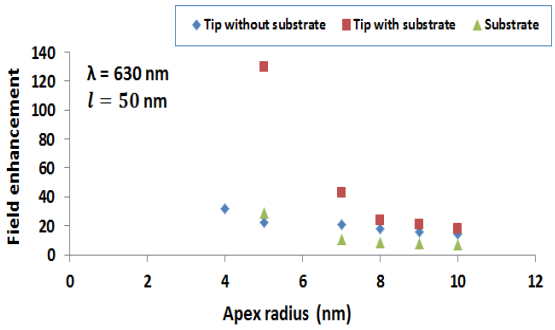

Figure 4 Dependence of field enhancement on the Au tip apex radius for the tip without substrate (blue) as well as the tip with the glass substrate (red) at a tip-sample distance of 5 nm with 630 nm illumination. Green shows the field at the substrate.

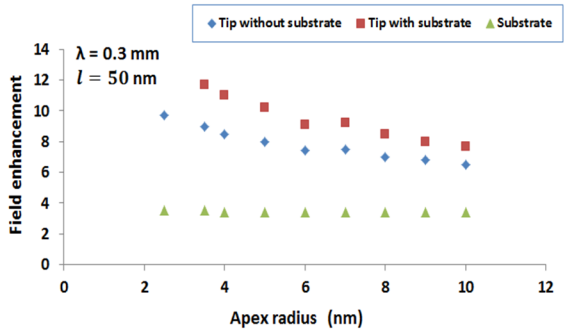

Figure 5 Dependence of field enhancement on the Au tip apex radius for the tip without substrate (blue) as well as tip with substrate (red) and at substrate (green) with tip-sample distance of 5 nm with 0.3 mm illumination.

On the other hand, at frequencies well below the metal plasma frequency (here, 1 THz), surface plasmons exhibit a very weak field confinement [18]. Thus, the dependence of the (weak) field enhancement on the Au tip apex radius is approximately linear (figure 5).

4.2 Competition between antenna and plasmon resonances and associated dephasing effects

Figure 6 and 7 show the field enhancement near the tip apex of the Au hemi-ellipsoid with the Au shaft added with a total height of L (figure 3) at

optical and THz regimes respectively. Our FEM calculations show that there is a maximum field enhancement due to plasmon resonance when $r = {}^{l_x}/_{l_y} = {}^{105\ nm}/_{53\ nm} \approx 2$ at $\lambda = 630$ nm.
The dephasing effects play an important role at a larger size L. Thus, the field enhancement drastically decreases when L is larger than 0.4 λ.

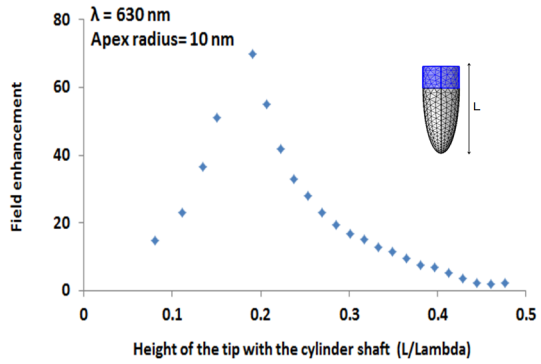

Figure 6 . Dependence of field enhancement γ on the height of the Au hemi-ellipsoid at $\lambda = 630$ nm. Field enhancement is increased due to plasmon resonance. When L is larger than 0.4 λ, field enhancement is less than 10 due to dephasing effects.

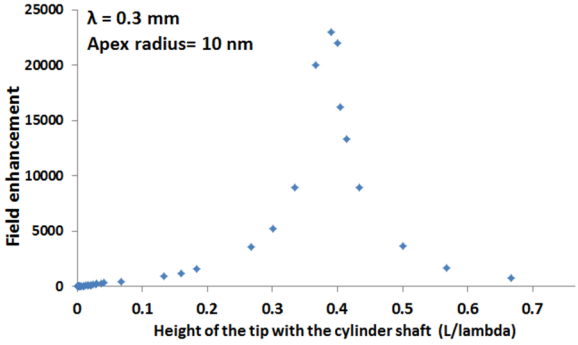

Figure 7. Dependence of field enhancement γ on the height of the Au hemi-ellipsoid at $\lambda = 0.3$ mm. Very large γ is due to antenna resonance at THz regime.

In contrast, THz frequencies cannot excite plasmon resonances. Thus, it is the antenna resonance which contributes to a strongly confined near field at the Au tip apex, leading to a maximum at close to 0.5 λ, This is expected as L is close to the antenna resonance condition of an odd integer multiple of half a wavelength. The reduction in field enhancement is due to the non-resonant antenna condition for these lengths. It is clear that for these large wavelengths the antenna effect is dominant and leads to an extremely high field enhancement.

7. Conclusion

We demonstrate the effect of two different underlying physical origins of the field enhancement at the end of a sharp tip by using FEM calculations. Our results are consistent with both analytical solutions and FETD calculations. At optical regime, dephasing effects can severely reduce the enhancement of electric field by modifying the plasmon resonance condition. The plasmon resonance is found for a gold hemi-ellipsoid when the aspect ratio is almost 2 ($\boldsymbol{r \approx 2}$). This is in good agreement with the recent publication for a gold full ellipsoid where the plasmon resonance is found for $\boldsymbol{r \approx 3.2 - 3.5}$. Furthermore, our results show non-linear dependence of the electric field enhancement on the apex radius of gold hemi-ellipsoid in the optical regime.
On the other hand, at THz frequencies the antenna effect is dominant, leading to high field enhancement. The dependence of the electric field enhancement on the apex radius is almost linear and reaches maxima at odd integer multiples of half a wavelength.

8. Acknowledgments:

We acknowledge financial support for this work from the Natural Sciences and Engineering Research Council of Canada (NSERC) as well as Fonds de recherche du Québec-Nature et technologies (FQRNT).

8. References

[1] A. J. Huber et al, Terahertz near-field nanoscopy of mobile carriers in single semiconductor nanodevices, Nano Letters, Vol. 8, No. 11, 3766-3770 (2008).
[2] Nastaran Kazemi et al, Localized enhancement of electric field in tip-enhanced Raman spectroscopy using radially and linearly polarized light, Opt. Express 21, 25271 (2013).

[3] K. Kneipp et al, Surface-Enhanced Raman Scattering, No. 3, Springer (2006)
[4] Nicolas Behr et al, Optical antenna properties of scanning probe tips: plasmonic light scattering, tip-sample coupling, and near-field enhancement, J. Phys. Chem. C, 112, 3766-3773 (2008).
[5] Anders Pors et al, Scaling in light scattering by sharp conical metal tips, Opt. Lett., Vol. 39, No. 11, 3308 (2014).
[6] A. Madrazo et al, Polarization effects in the optical interaction between a nanoparticle and a corrugated surface: implications for apertureless near field microscopy, J. Opt. Soc. Am. A, Vol. 15, No. 1, 109 (1998).
[7] Olivier J et al, Controlling and tuning strong optical field gradients at a local probe microscope tip apex, Appl. Phys. Lett, 70, 6 (1997).
[8] Radouance Fikri et al, Apertureless scanning near field optical microscopy: the need for probe-vibration modeling, Opt. Lett, Vol.28, No. 22, 2147 (2003).
[9] J. A. Porto, Resonance shift effects in apertureless scanning near field optical microscopy, Phys. Rev. B 67, 085409 (2003).
[10] Christoph Huber et al, Optical near-field excitation at commercial scanning probe microscopy tips: a theoretical and experimental investigation, Phys. Chem. Chem. Phys., 16, 2289 (2014).
[11] Wan-Xin, Ze-Xiang, Optimizing the near field around silver tips, J. Opt. Soc. Am. A., Vol. 20, No. 12, 2254 (2003).
[12] W. Hergert, T. Wriedt, The Mie theory, Springer (2012).
[13] Andrew Downes et al, Finite element simulations of tip-enhanced Raman and fluorescence spectroscopy, J. Phys. Chem. B, 110, 6692-6698 (2006).
[14] Yves C. Martin et al, Strength of the electric field in apertureless near-field microscopy, J. app. phys, Vol. 89, No. 10, 5774 (2001).
[15] Warren L. Stutzman, Gary A. Thiele, Antenna Theory and design 3rd ed, John Wiley & sons, Inc, (2012).
[16] J. Jersch et al, Field enhancement of optical radiation in the near field of scanning probe microscope tips, Appl. Phys. A 66, 29-34 (1998).
[17] Handbook of terahertz technology for imaging, sensing and communications, Woodhead publishing (2013).
[18] T. H. Isaac et al, Determining the terahertz optical properties of subwavelength films using semiconductor surface plasmons, App. Phys. Let. 93, 241115 (2008).